



Article

Synthesis of Tribological WS₂ Powder from WO₃ Prepared by Ultrasonic Spray Pyrolysis (USP)

Nataša Gajić ^{1,*}, Željko Kamberović ², Zoran Anđić ³ , Jarmila Trpčevská ⁴,
Beatrice Plešingerova ⁴ and Marija Korać ² 

¹ Innovation Center of the Faculty of Technology and Metallurgy in Belgrade Ltd., University of Belgrade, Karnegijeva 4, 11120 Belgrade, Serbia

² Faculty of Technology and Metallurgy, University of Belgrade, Karnegijeva 4, 11120 Belgrade, Serbia; kamber@tmf.bg.ac.rs (Ž.K.); marijakorac@tmf.bg.ac.rs (M.K.)

³ Innovation Center of the Faculty of Chemistry in Belgrade Ltd., University of Belgrade, Studentski trg 12-16, 11000 Belgrade, Serbia; zoranandjic@yahoo.com

⁴ Faculty of Materials, Metallurgy and Recycling, Technical University of Košice, Letná 9, 042 00 Košice, Slovensko; jarmila.trpcevska@tuke.sk (J.T.); beatrice.plesingerova@tuke.sk (B.P.)

* Correspondence: ngajic@tmf.bg.ac.rs; Tel.: +381-605-236-021

Received: 30 December 2018; Accepted: 22 February 2019; Published: 28 February 2019



Abstract: This paper describes the synthesis of tungsten disulfide (WS₂) powder by the sulfurization of tungsten trioxide (WO₃) particles in the presence of additive potassium carbonate (K₂CO₃) in nitrogen (N₂) atmosphere, first at lower temperature (200 °C) and followed by reduction at higher temperature (900 °C). In addition, the ultrasonic spray pyrolysis of ammonium meta-tungstate hydrate (AMT) was used for the production of WO₃ particles at 650 °C in air. The HSC Chemistry[®] software package 9.0 was used for the analysis of chemistry and thermodynamic parameters of the processes for WS₂ powder synthesis. The crystalline structure and phase composition of all synthesized powders were analyzed by X-ray diffraction (XRD) measurements. The morphology and chemical composition of these samples were examined by scanning electron microscopy (SEM) combined with energy dispersive X-ray analysis (EDX).

Keywords: tribology materials; tungsten disulfide; ultrasonic spray pyrolysis; tungsten trioxide

1. Introduction

According to current studies, nearly one-quarter of the world's total energy consumption originates from tribological contacts [1]. By improving the performance of current tribological materials, energy losses due to friction and wear could potentially be reduced by 40% in the long term (15 years) and by 18% in the short term (8 years) [1]. Hence, in the face of increasing global requirements for saving energy, there is no doubt that the search for efficient tribological materials with improved performances will continue in the coming years because the application conditions of future tribomechanical systems will undoubtedly be much more demanding than the current ones [2]. Today's market of tribological materials has unique requirements for the release of harmful substances (Cd, Pb, Cr, etc.) and the prevention of their migration into the environment during their use [3]. It is generally considered that these elements and their compounds, which can be introduced into food or water, are difficult to eliminate from the body and according to current studies can have carcinogenic effects [4]. For all of the above reasons, despite their excellent performances, tribological materials must also be acceptable from economic and ecological points of view. Among the various tribological materials, WS₂ has attracted a large amount of attention from researchers for its specific properties and extensive promising applications [5]. Even in small quantities, WS₂ contributes to the high performance of tribological

materials and their specific properties (chemical stability in a wide temperature range, the possibility of revitalizing the surface that they protect, they are corrosion-resistant, inert, non-toxic, non-magnetic, and have lamellar structure, low shear strength, high oxidation and thermal degradation resistance, and so forth), which are of particular importance for the functioning of modern tribomechanical systems. WS_2 is applicable in various types of industries, such as automotive, aerospace, military, medical, and so forth.

WS_2 crystals have a hexagonal structure composed of a layer of tungsten atoms packed in between two layers of sulfur atoms, as shown in Figure 1a. The bonding between W-S layers is very strong and covalent, but layers of S atoms are loosely bound through weak van der Waals forces. This structure is responsible for the interlayer mechanical weakness with low shear strength, which results in a macroscopic lubricating effect. Figure 1b shows the lubrication mechanism of WS_2 single sheets.

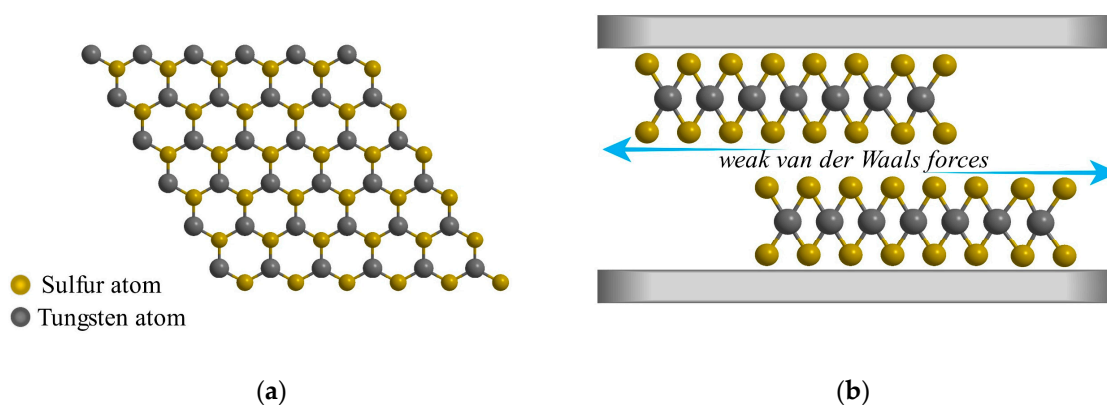


Figure 1. (a) Hexagonal structure of WS_2 (top view); (b) The relative sliding between two single layers of WS_2 (slide view).

So far, various methods of producing WS_2 of different size and morphology using WO_3 as precursor have been established, such as: gas–solid phase reaction [6–8], chemical vapor deposition (CVD) [9–11], hydrothermal method [12–14], mechanochemical activation method [15], and solid–solid phase reaction [16–18].

Gas–solid reactions present a very simple approach to generating WS_2 . In most cases, WO_3 is reacted with a sulfur-containing compound for extended periods of time at high temperatures. For example, WS_2 has been synthesized in a tubular furnace through gas phase reactions between WO_3 particles and H_2/H_2S gases at a temperature of 840 °C for 30 min in Ar gas flow [6], by sulfidation of hexagonal WO_3 with H_2S/H_2 (15% H_2S) at different temperatures: 400, 500, and 800 °C for 4 h [7], and by sulfurization of WO_3 nanostructured thin film in a mixture of H_2S and Ar gas (10:90) at different partial pressure values [8]. However, this method involves exposure to extremely toxic and harmful H_2S at elevated temperatures.

WS_2 flakes have been synthesized successfully on SiO_2/Si substrate by the sulfuration of WO_3 powder at high temperatures by the CVD method [9–11]. Furthermore, there was no poisonous H_2S gas released during these experiments and WS_2 of a high purity was obtained. Although this method has many advantages, it is very demanding to coordinate the complicated relations among many process parameters.

Using the hydrothermal method [12–14], WS_2 has been synthesized by autoclaving a mixture of WO_3 and sulfur precursor, followed by washing and drying of the resulting product. Although various inexpensive precursors can be used for this method, the productivity of this process is low and additional thermal treatment is necessary because the obtained WS_2 has an amorphous structure.

Wu Z. et al. [15] have synthesized WS_2 nanosheets by novel mechanochemical activation methods in which a ball-milled mixture of WO_3 and S powder was annealed at 600 °C for 2 h in an atmosphere of Ar gas. This method seems to be environmentally advantageous and may be an alternative to the traditional route of synthesis, but it is a very complex process and a robust method for the production

of particles with small dimension. Another difficulty arises from the fact that there is still a lack of clear interpretation of the exact reaction and activation mechanism.

Regarding solid–solid phase reaction, the synthesis of WS_2 powder was carried out by sulfurization of the WO_3 powder with thiourea in a N_2 atmosphere at 850 °C for 1 h in a horizontal tube furnace [16–18].

In this investigation the sulfurization of the WO_3 particles with S powder in the presence of additive K_2CO_3 in a nitrogen atmosphere was studied. In order to obtain an adequate precursor for synthesis, this research involved the production of WO_3 particles using an ultrasonic spray pyrolysis method. It is a simple and low-cost method, which in continuous operation can generate spherical, non-agglomerated submicron particles by using commercially available (inexpensive) precursors [19]. The as-prepared WO_3 particles were used for WS_2 synthesis without any post processing because they were free of impurities.

2. Experimental

2.1. Materials and Methods

The raw materials used for the experimental test performed in this work were: WO_3 obtained by ultrasonic spray pyrolysis (USP), commercial WO_3 (Chemapol, Prague, Czech Republic), sulfur (Solvay & CPC Barium Strontium GmbH & Co, Hannover, Germany, powder with characteristic size <45 μm , purity 99.95%), and K_2CO_3 (Zorka, Šabac, Serbia). Commercially available WS_2 powder (SpeedUP INTERNATIONAL, Belgrade, Serbia, with a minimum 99.4% WS_2 and WO_3) was used for comparative analysis. The production of precursor, WO_3 powder, as well as the synthesis of WS_2 powders were carried out in a rotary tilting tube furnace (ST-1200RGV).

The HSC Chemistry[®] software package 9.0 was used for the analysis of the chemistry and thermodynamic parameters of the processes for the synthesis of WS_2 powder [20]. The determination of appropriate conditions for WS_2 synthesis was crucial for this analysis. Therefore, the Gibbs free energy of theoretically suspected chemical reactions during the WS_2 synthesis process, the phase stability diagram for the W–O–S system, and the equilibrium composition of the species in the WO_3 –S– K_2CO_3 system were calculated using HSC Chemistry software.

All obtained powders, as well as the commercial WS_2 powder, were subjected to analysis on a scanning electron microscope (SEM) equipped with energy dispersive X-ray analysis (EDX), a MIRA FE-SEM, from TESCAN Inc. In SEM images of the WO_3 powder, well-dispersed powder without any agglomerates was clearly seen and the determination of particle size distribution for the WO_3 powder was done using the Image Pro Plus Software. However, the particle size of the WS_2 powder was not identifiable using image analysis due to the poor dispersion of samples. Size measurements of the obtained WS_2 powders were thus performed using a laser particle size analyzer (Malvern Instruments, Malvern, UK). In addition, all samples were subjected to X-ray diffraction analyses using a Philips PW 1710, X-Pert Pro diffractometer (Co $K\alpha$ radiation, generated at 40 kV and 30 mA). Measurements were carried out at an angle interval $10^\circ < 2\theta < 119^\circ$ with step 0.017° . XRD results were analyzed by employing the Rietveld method with the help of PowderCell Software and the RIFRANE[®] programme.

2.2. Synthesis of WO_3 Powder

The apparatus for WO_3 synthesis consisted of an aerosol generator (“Profi Sonic”, Prizma, Kragujevac), a horizontal reactor with a quartz glass tube (0.5 m diameter and 1.2 m length), a vacuum pump (VP125), and powder collectors (Figure 2).

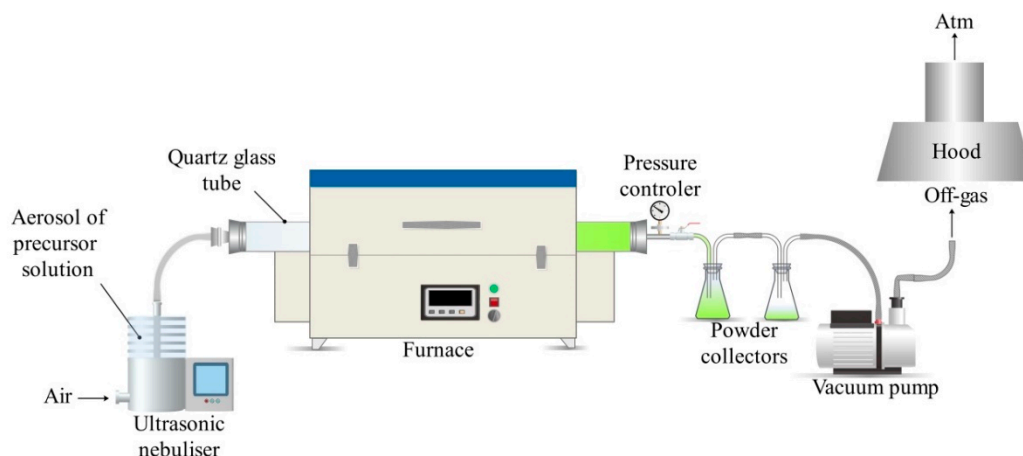
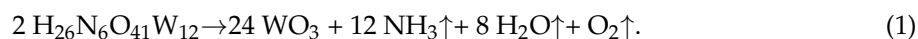


Figure 2. Schematic illustration of experimental setup for the ultrasonic spray pyrolysis (USP) synthesis of WO_3 .

Firstly, the ammonium meta-tungstate hydrate ($\text{AMT}—\text{H}_{26}\text{N}_6\text{O}_{41}\text{W}_{12}\cdot\text{aq}$) diluted in distilled water was put into the particle nebulizer to generate an aerosol. The concentration of AMT solution was 10 mmol/L. For this ultrasonic nebulizer system, the resonance frequency was set to 1.7 MHz. A vacuum pump and air with a flow rate of 5 L/min was used to introduce the generated aerosol droplets into the tubular reactor. Prior to the introduction, the temperature of the reactor was raised to 650 °C. The pressure of the system was adjusted using the reactor pressure controller. The calculated retention time of droplets in the reaction zone was estimated to be about one second. After thermal decomposition of the transported aerosol in the furnace, the formed WO_3 was partially collected in the bottles with water and alcohol. During the spray pyrolysis process, the evaporation of water from aerosol droplets increases the concentration of AMT in the droplets. Finally, AMT is thermally decomposed according to Equation (1):



As shown in Figure 3, the mechanism of WO_3 particle formation proposed by Arutanti et al. [21] is comprised of different steps starting from an initial solution of AMT.

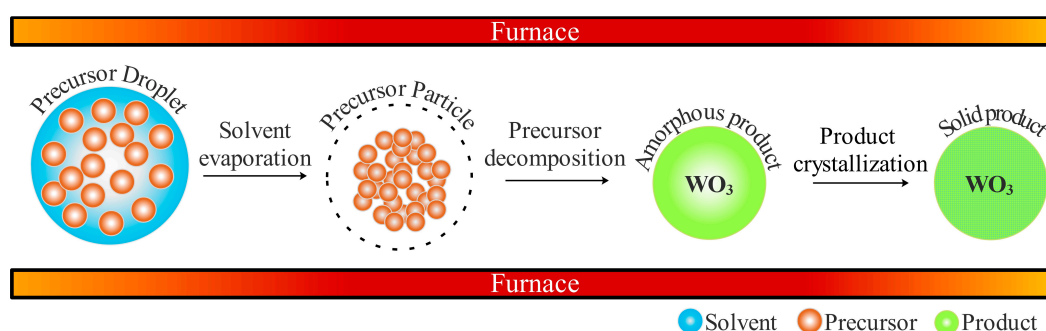


Figure 3. The mechanism of the formation of WO_3 particles in the spray pyrolysis method.

2.3. Synthesis of WS_2 Powder

A schematic illustration of the WS_2 synthesis process is shown in Figure 4.

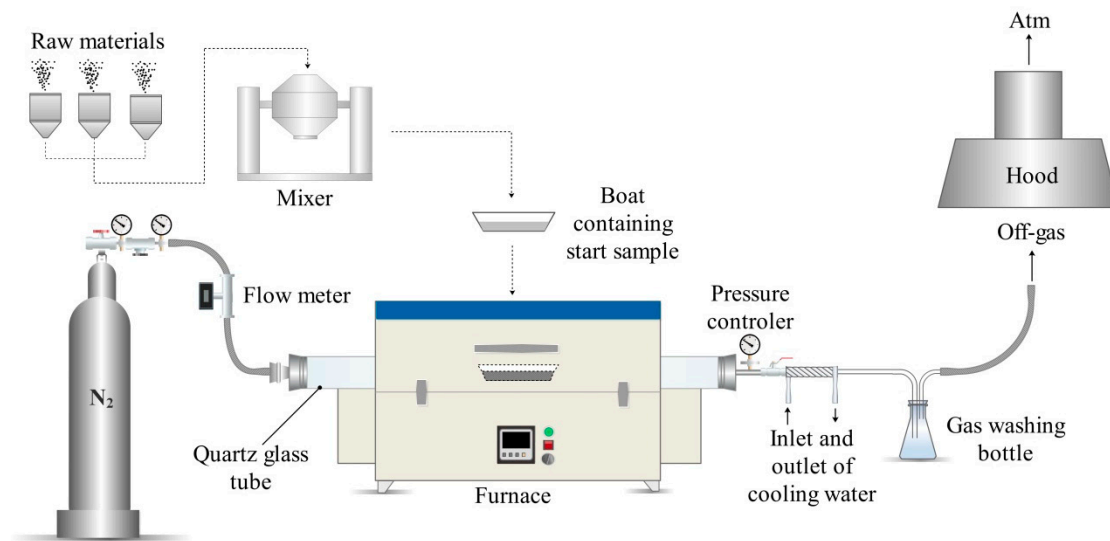


Figure 4. Schematic illustration of the experimental setup for the synthesis of WS₂ powder.

K₂CO₃ powder (5 wt.%) was added to the WO₃ and S powder mixture with a weight ratio of 60:40. The powders were mixed and ground for 15 min in the mixer. Then, the as-prepared mixture was transferred to a covered ceramic boat. The boat was placed in the center of the quartz tube and into the furnace. High-purity nitrogen gas was introduced through one side of the furnace, whilst the other side of the quartz tube was connected to a cooling system and outlet gas washing system. The total flow rate of the N₂ gas was fixed at 200 cm³·min⁻¹ for all experimental conditions. Prior to heating the furnace, nitrogen gas was flushed constantly for about 30 minutes to remove residual air in the furnace. First, the furnace with the sample was heated at a lower temperature (200 °C) at a rate of 10 °C/min and maintained under these conditions for 2 h. Then, it was further heated at a rate of 5 °C/min followed by reduction at a higher temperature (900 °C). After 2 h, the furnace was turned off and allowed to cool down to room temperature. Nitrogen gas flow was stopped and the WS₂ powder was collected from the boat.

3. Result and Discussion

3.1. Thermodynamic Analysis

Results of the thermodynamic analysis of the process of WS₂ powder synthesis are discussed below. Using the assumption of raw materials for the composition of the synthesis process, the following chemical reactions (Equations (2)–(4)) were considered:

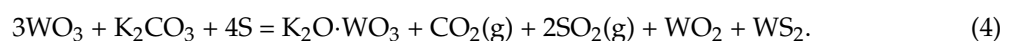
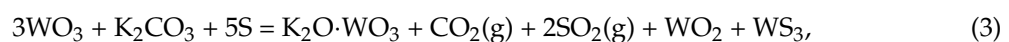
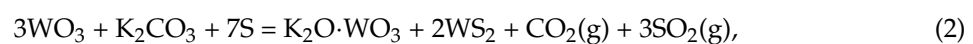


Figure 5 shows the calculated results of the Gibbs energy of reactions versus temperature from the reaction of Equations (2)–(4). The temperature range that was considered was up to 1000 °C.

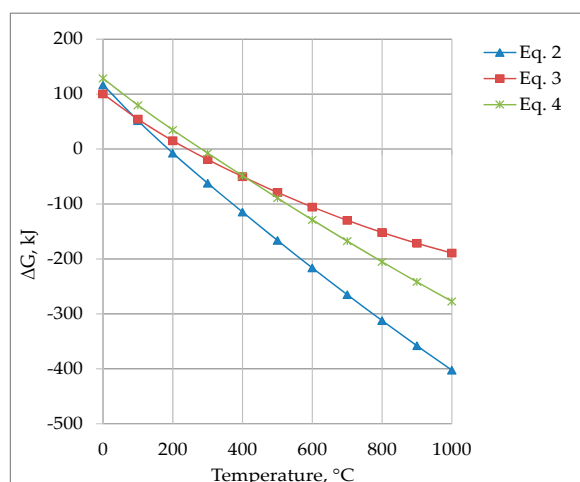


Figure 5. The change in Gibbs free energy (ΔG) versus temperature for the different possible reactions that take place during the WS_2 synthesis.

As shown in Figure 5, it can be clearly seen that the ΔG of all reactions has a negative value at temperatures higher than 300 °C, which means that all of the reactions are theoretically possible from the thermodynamic point of view. However, among them, the changes of the Gibbs energy of reaction presented with Equation (2) has a more negative value relative to Equations (3) and (4) (i.e., Equation (2) is dominant).

The equilibrium composition of the WO_3 – K_2CO_3 – S system at different temperatures was calculated using the HSC computer program based on the Gibbs energy minimization method, and the results are shown in Figure 6.

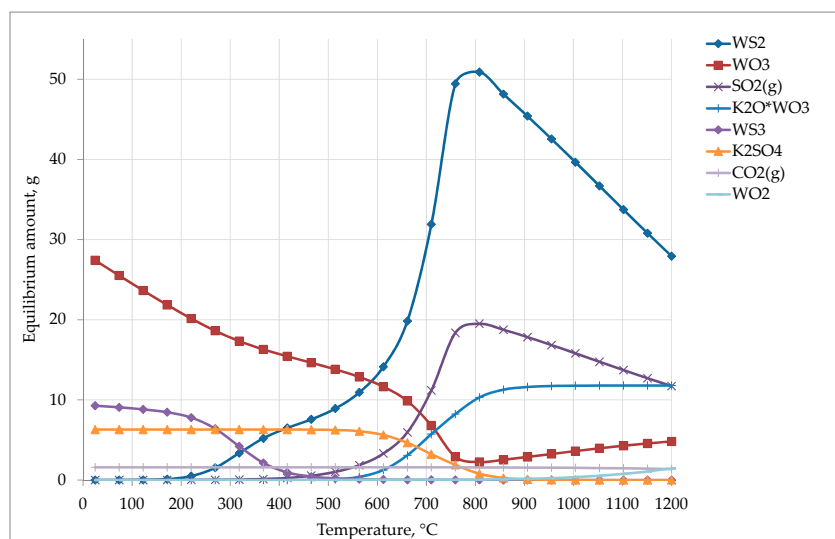


Figure 6. Equilibrium amount of WO_3 – S – K_2CO_3 reactant system in N_2 gas atmosphere.

The highest stability of WS_2 was achieved at approximately 800 °C when the stability of the reactants were decreasing. $K_2O \cdot WO_3$ and WO_2 phases also became stable at the same temperature. The main gaseous products of this reaction were gaseous SO_2 and CO_2 .

In the analyzed system, the main products of the reactions at a temperature of 900 °C were WS_2 , $K_2O \cdot WO_3$, WO_2 , CO_2 , and SO_2 . These results were only qualitative.

By using thermodynamic software, a phase stability diagram for the W – O – S system for constant partial pressure of oxygen was constructed (Figure 7).

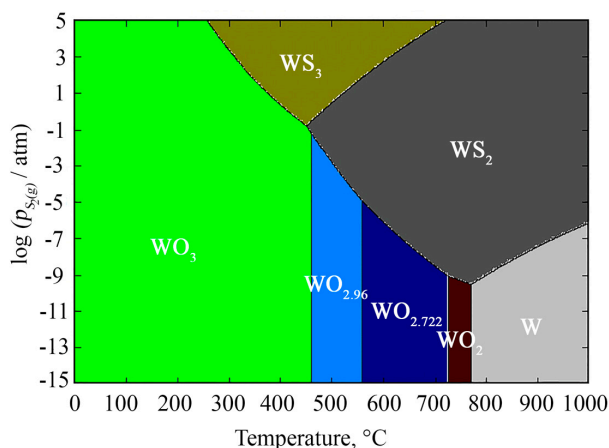


Figure 7. Temperature–partial pressures (Tpp) phase stability diagram for the W–O–S system at constant oxygen partial pressure.

Considering the logarithmic sulfur vapor pressure of 1 atm [22] and experimental temperature of 900 °C, it was found that the predominant stability area was of WS_2 . At these temperatures, the vapor pressure of sulfur is such that it led to the saturation of the atmosphere with the sulfur vapor in the furnace. This meant that the amount of sulfur gas phase necessary to react with the WO_3 was sufficient to establish contact between the mentioned phases. Further, the diffusion of sulfur into WO_3 was enabled to form WS_2 powder.

The synthesis of WS_2 was performed in two stages: (i) initiation of synthesis at a low temperature (200 °C) followed by (ii) high-temperature (900 °C) reduction. The temperature of the first stage was selected to prolong the contact time of sulfur and WO_3 in the starting powder mixture, before sulfur self-ignition (232 °C) which promotes the transformation of sulfur to a gas phase and the evaporation of a large amount of S and/or SO_2 . This loss of sulfur obstructs its diffusion into WO_3 and consequently obstructs the synthesis of WS_2 . Thermodynamic analysis of the second stage indicated that the optimal temperature of the synthesis was above 800 °C. However, at lower temperatures oxides were formed and the chemical composition of the mixture was changed, and a lower level of crystallization occurred.

For that reason, the second stage of synthesis was carried out at 900 °C to prevent oxide formation and to increase the degree of crystallinity in the final WS_2 product.

3.2. Characterization of Synthesized WO_3 Powder

Figure 8a,b shows the SEM images of the synthesized WO_3 powder by USP method under different magnifications. The result of EDX analyses from the presented scanning surface is given in Figure 8c, which reveals that the sample consisted of the elements tungsten and oxygen, and no other elements were observed.

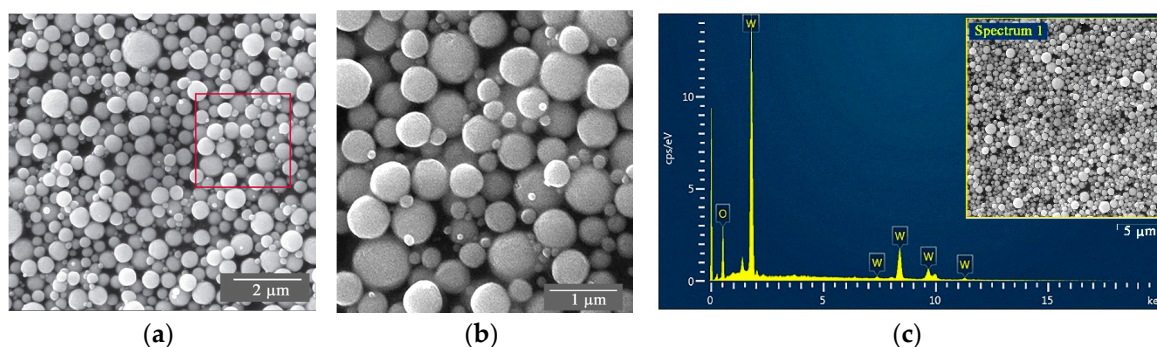


Figure 8. (a,b) SEM images and (c) EDX spectrum of WO_3 powder synthesized by USP.

The XRD pattern of the prepared WO₃ particles is shown in Figure 9. It is evident from the pattern that no diffraction peaks from other elements of compounds were found in the samples. Therefore, it is obvious that the as-prepared samples were composed of WO₃. The XRD pattern suggested that the prepared particles had two types of crystal structures: hexagonal and monoclinic.

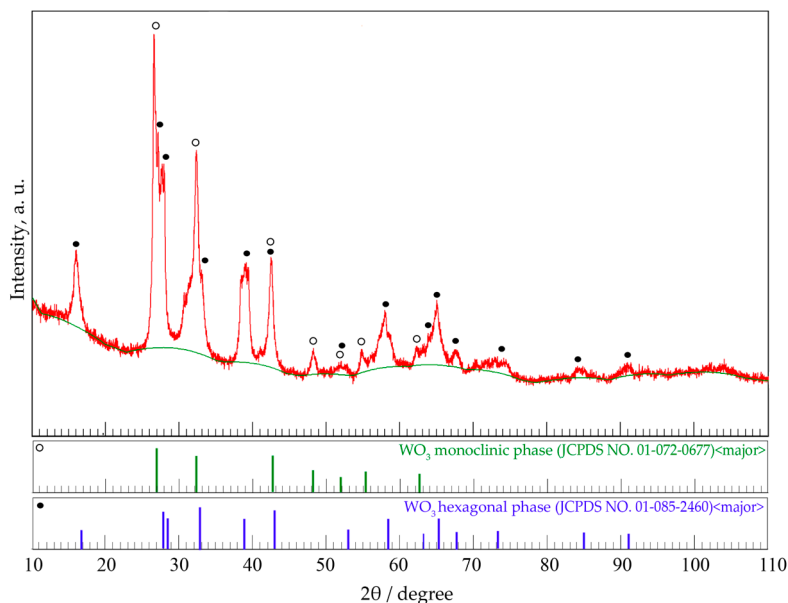


Figure 9. XRD pattern of WO₃ powder prepared by USP method.

The particle size distribution determination for the WO₃ powder prepared by USP is presented in Figure 10.

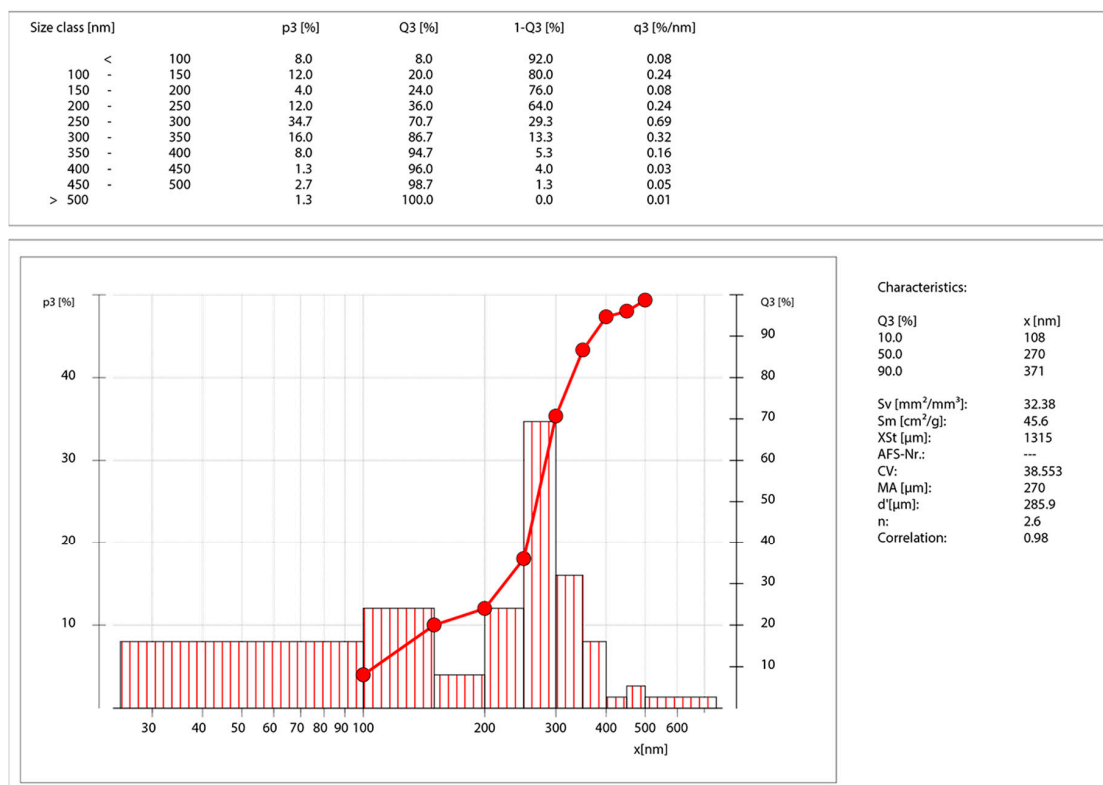


Figure 10. Particle size distribution for WO₃ powder prepared by USP method.

3.3. Characterization of WS₂ Powder

Figure 11a demonstrates an SEM image of powder obtained using the WO₃ precursor powder prepared by the USP method. The sample was composed of a large number of ultrathin WS₂ flakes. Furthermore, WO₂, WO₃, and K₂O·WO₃ phases with larger dimensions of particles were noticeable. The structure of the ultrathin flakes from the marked locations is presented more clearly in Figure 11b. The results demonstrate the presence of flower-shaped WS₂ particles composed of nanoflakes of 200–500 nm in length and 50 nm in mean thickness. A further EDX analysis of the sample presented in Figure 11c reveals that the product was composed of W, S, O, and K, which suggests that the powder was composed of mainly WS₂ (Spectrum 1) and WO₂, WO₃, and K₂O·WO₃ (Spectrum 2) phases, in accordance with the results presented in Figure 6.

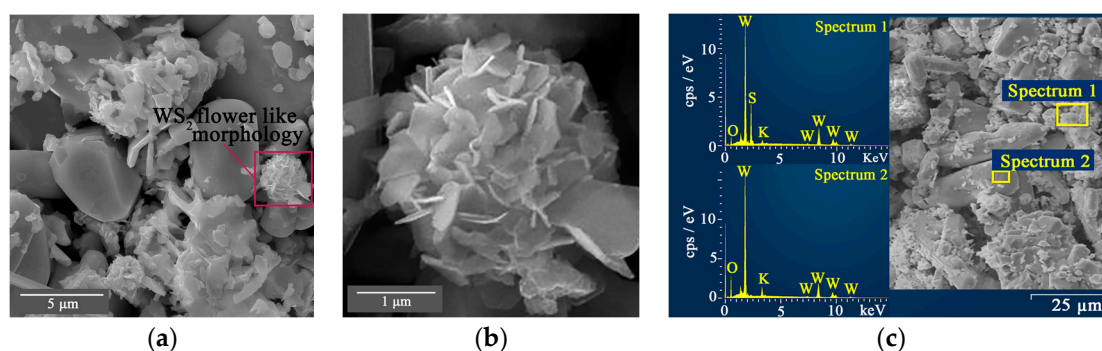


Figure 11. (a,b) SEM images and (c) EDX spectrum for WS₂ synthesized using WO₃ prepared by USP as precursor.

The results of the XRD analysis employing the Rietveld method are shown in Figure 12. These results revealed that WS₂ phase was predominant (present in two crystallized forms: hexagonal and rhombohedral) and was accompanied by the presence of WO₂ (9.80%), WO₃ (3.04%), and K₂O·WO₃ (1.56%) phases.

The obtained WS₂ particles were tested for their size and size distribution and the mean particle size was found to be around 950 nm (Figure 13).

WS₂ powder synthesized using WO₃ prepared by USP as precursor was selected as a lubrication additive in SF SAE 15W-40 motor oil. WS₂ powder was ultrasonically dispersed into the base oil for 10 min. In addition, a base oil without any additive was also prepared. Wear tests were conducted using a ball-on-disc configuration on a Bruker UMT-3 tribometer (Bruker, Billerica, MA, USA). This test method involves a ball-shaped upper specimen that slides against a rotating disk as a lower specimen under a prescribed set of conditions. Both the ball and the steel disc were cleaned with acetone and dried with a normal stream of air before the test. A normal load of 50 N and a linear sliding speed of 0.1 m/s were used for the experiments, for a sliding distance of 500 m. The results of base oil with additive showed that the average value of the friction coefficient was $\mu \sim 0.1$. It was concluded that the friction coefficient of the base oil ($\mu \sim 0.16$) was improved by adding WS₂. The mass ratio of WS₂/base oil in samples was 1.0 wt.%.

The generated WS₂ powder had plate-like particles, which were oriented differently when the starting material was commercial WO₃ powder (Figure 14a). It can also be clearly seen from Figure 14b that WS₂ particles were clustered together and exhibited evident agglomeration of up to 1 μm in size. The thickness of the WS₂ plate-like particles was approximately 100 nm and their lengths varied from 500 nm to 1 μm. Results of EDX analyses from marked locations showed the presence of W and S elements and a certain content of O and K elements which indicated the presence of WS₂ (Spectrum 2) and WO₂, WO₃, and K₂O·WO₃ (Spectrum 1) phases (Figure 14c).

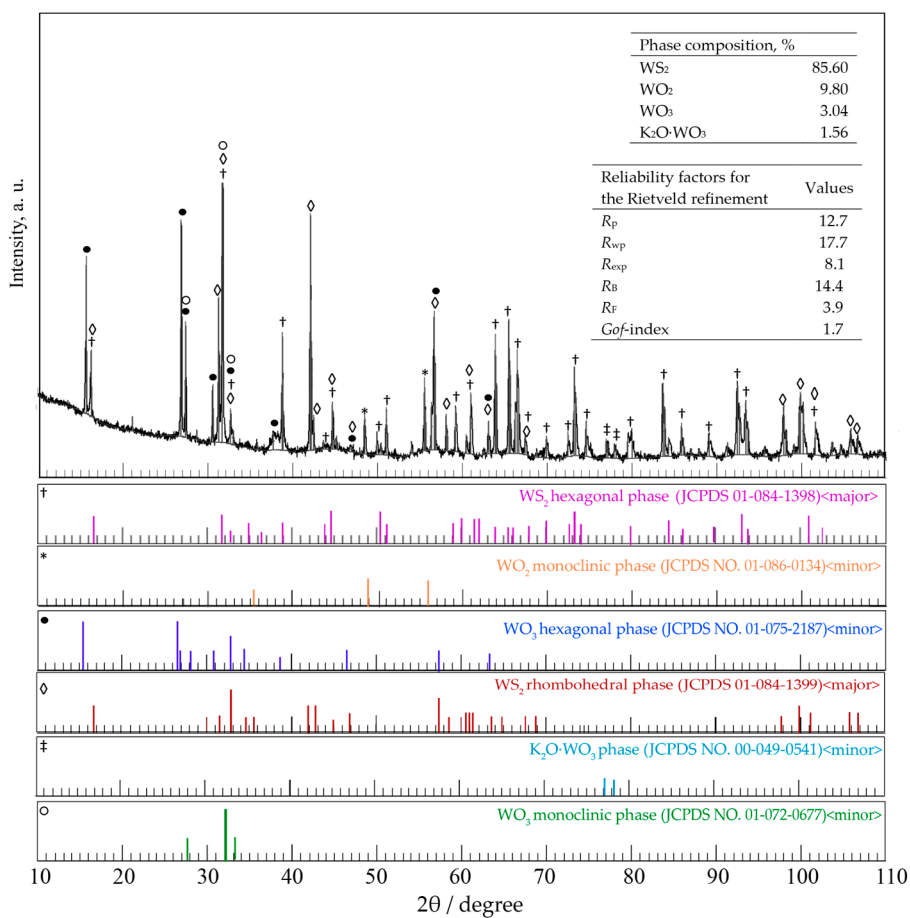


Figure 12. XRD pattern of WS₂ synthesized using WO₃ prepared by USP as precursor.

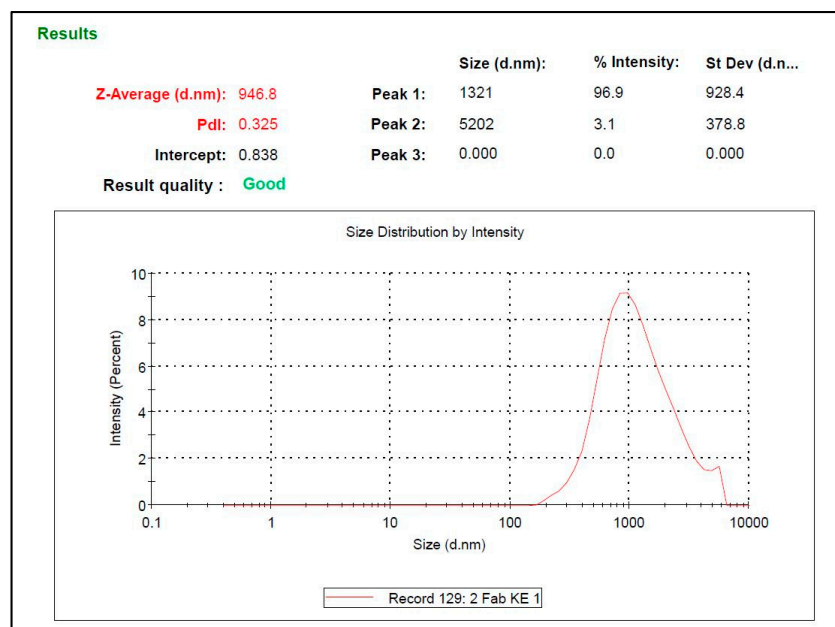


Figure 13. Particle size distribution by intensity of WS₂ particles synthesized using WO₃ prepared by USP as precursor.

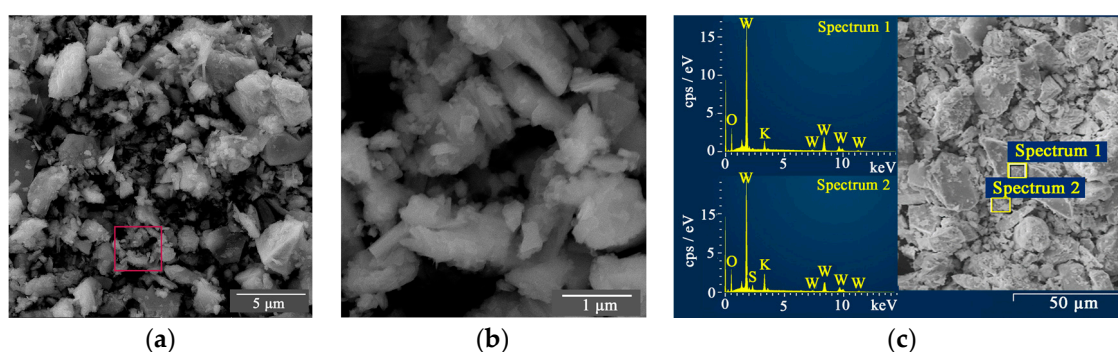


Figure 14. (a,b) SEM images and (c) EDX spectrum for WS_2 synthesized using commercial WO_3 as precursor.

The sample of WS_2 powder synthesized using commercial WO_3 as precursor was analyzed by XRD (Figure 15). Results showed the predominance of the WS_2 phase, present in two crystallized forms: hexagonal and rhombohedral. WO_3 , WO_2 , $K_2O \cdot WO_3$, and S phases were also identified, of which WO_3 was hexagonal and monoclinic. The strong and sharp diffraction peaks in the pattern indicated that the product was very highly crystallized.

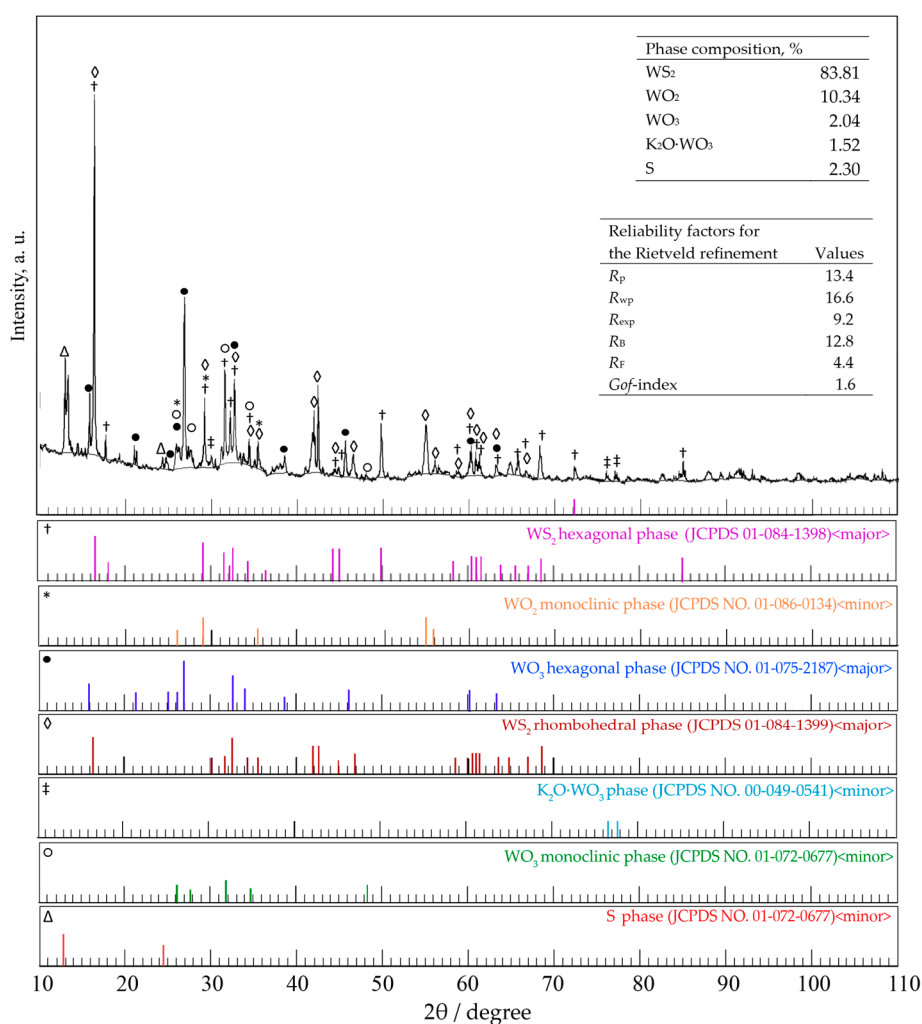


Figure 15. XRD pattern of WS_2 synthesized using commercial WO_3 as precursor.

The obtained WS₂ particles were tested for their size and size distribution and the mean particle size was found to be around 500 nm (Figure 16).

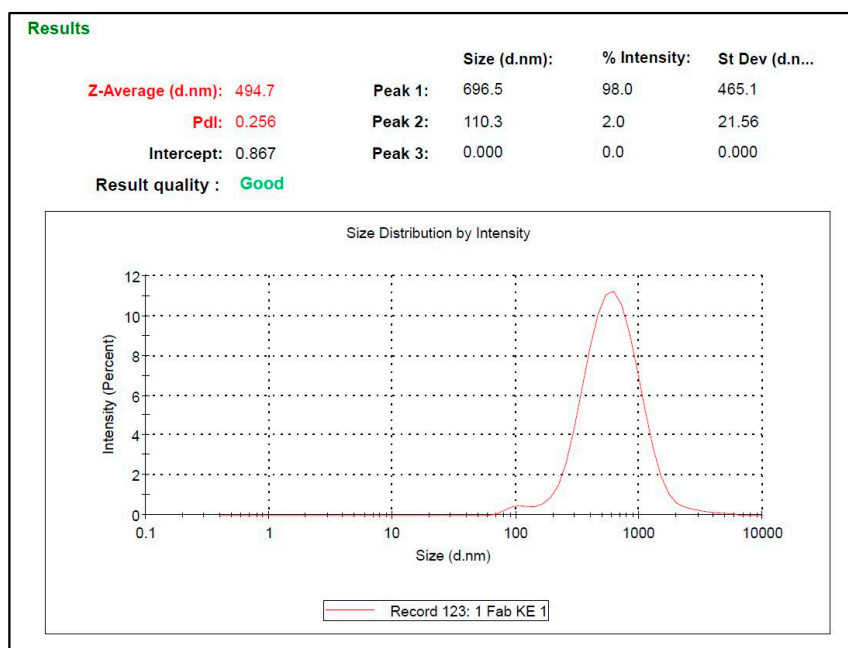


Figure 16. Particle size distribution by intensity of WS₂ particles synthesized using commercial WO₃ powder as precursor.

Commercial WS₂ powder as evidenced by SEM images consisted of nanoparticles with the presence of large agglomerates (Figure 17a). The uniform shape of particles can be seen in Figure 17b. On the basis of the EDX analysis as well as the high content of W and S, the presence of O was also confirmed (Figure 17c).

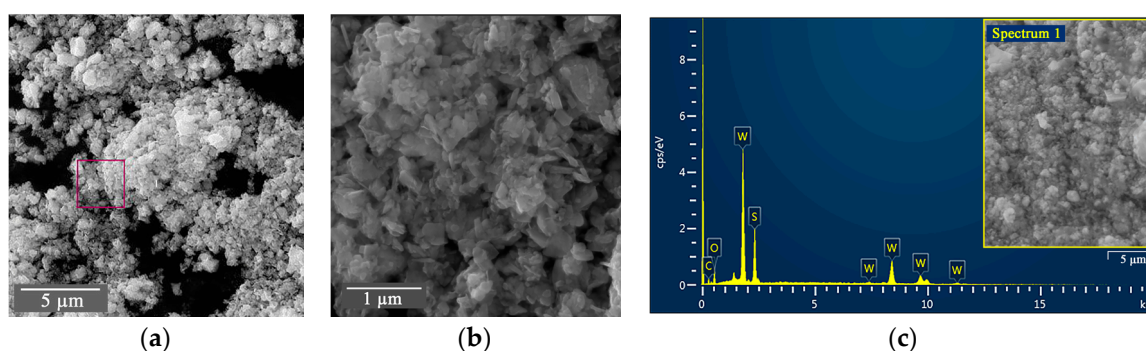


Figure 17. (a,b) SEM images and (c) EDX spectrum for commercial WS₂.

The XRD analysis of the commercial WS₂ powder indicated that there were major WS₂ and WO₃ phases and a minor WO₃·0.33H₂O phase, with low levels of crystallinity (Figure 18c). The presence of the amorphous phase was dominant, although the crystalline phase was also present.

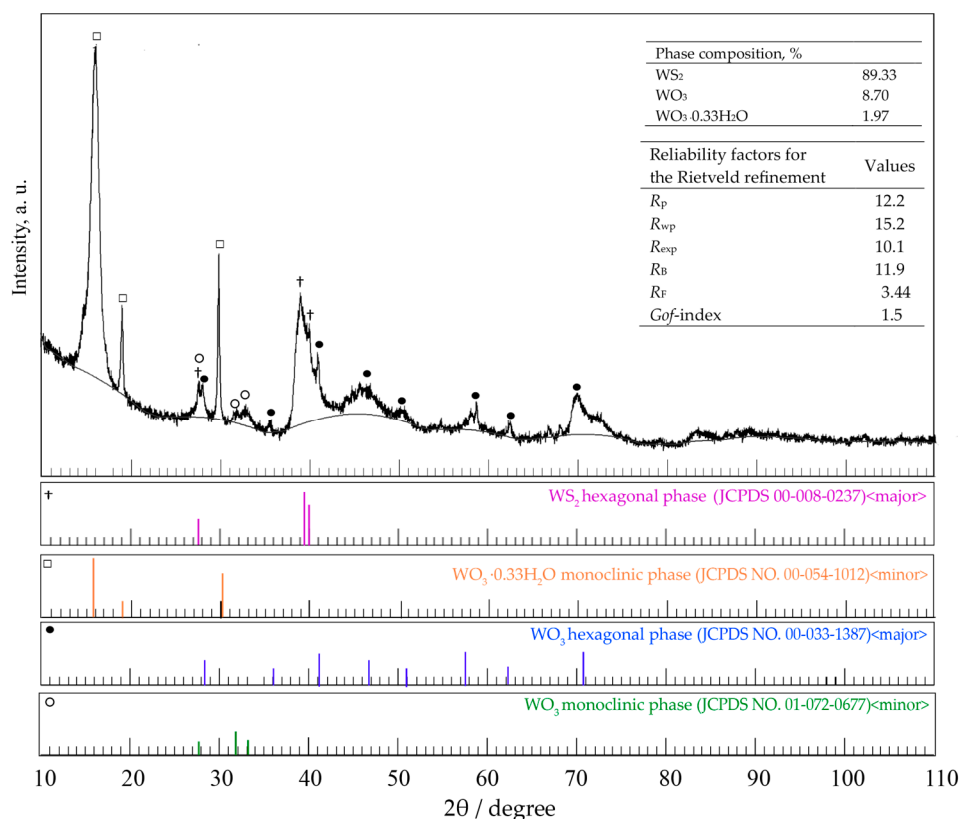


Figure 18. XRD pattern of commercial WS₂ powder.

Comparative analysis of the obtained powders with commercial WS₂ powder showed differences in particle size and agglomerates. The commercial WS₂ powder had the smallest particle size, but had more agglomerates compared to synthesized powders. Agglomerated powders are not good for tribological properties [23].

Particles of the synthesized WS₂ powders ranged from submicrometers to micrometers in size. The mixture of these two powders should provide better friction and wear performance between contacting surfaces, according to N. Wu et al [24].

Apart from the presence of sulfide as the main product, commercial WS₂ powders had a WO₃ (8.70%) phase, whereas synthesized WS₂ powders had K₂O·WO₃ (1.52–1.56%), WO₂ (9.80–10.34%), and WO₃ (2.04–3.04%) phases. In order to obtain WS₂ powders that will provide low and stable friction coefficients, the presence of WO₃ should be avoided [25]. In synthesized powders, the WO₃ phase was less abundant relative to the levels found in commercial WS₂ powders. Both tungsten dioxides and tungsten disulfides exhibited similar lubrication performances [26]. The materials with low oxygen content were more resistant to wear [27]. In this respect, WO₂ in synthesized WS₂ powders led to a lower friction coefficient. In addition, the K₂O·WO₃ phase in synthesized powders improved the thermal stability of obtained WS₂ powders [28].

4. Conclusions

In response to the requirements for improving performances of currently available tribological materials, this work demonstrated the synthesis of WS₂ powder using ultrafine WO₃ powder prepared by USP method. In addition, we synthesized WS₂ powder using commercial WO₃ powder as precursor.

The synthesis of WS₂ powder with the addition of K₂CO₃ as a fluxing agent reduced the WO₃ precursor and protected the sample against oxidation, which is one of the advantages of the applied method.

Further, the results of the XRD analysis of synthesized powders were in accordance with thermodynamic predictions. In the synthesized WS₂ powders, K₂O·WO₃ and WO₂ phases were present in addition to the WS₂ phase. These phases are useful from the aspect of thermal stability and friction coefficient control of the powders.

As a result of this investigation, two sizes of WS₂ particles ranging from submicrometers to micrometers were obtained. Hence, future efforts are planned to investigate mixed micro/submicron lubrication systems composed of the synthesized WS₂ powders.

In summary, tribological WS₂ powder was successfully prepared by a facile and environment-friendly method.

Author Contributions: Conceptualization, Ž.K.; Formal analysis, J.T.; Investigation, N.G.; Methodology, Ž.K. and Z.A.; Resources, M.K.; Software, N.G. and B.P.; Supervision, Ž.A.; Validation, J.T. and B.P.; Writing—original draft, Ž.K.; Writing—review & editing, M.K.

Funding: This research was funded by the Ministry of Education, Science and Technological Development of the Republic of Serbia, project No. 34033.

Acknowledgments: This paper was done with the financial support of the Ministry of Education, Science and Technological Development of the Republic of Serbia and it is a result of project No. 34033.

Conflicts of Interest: The authors declare no conflict of interest.

References

1. Holmberg, K.; Erdemir, A. Influence of tribology on global energy consumption, costs and emissions. *Friction* **2017**, *5*, 263–284. [[CrossRef](#)]
2. Stojanović, B.; Ivanović, L. Tribomechanical systems in design. *J. Balk. Tribol. Assoc.* **2014**, *20*, 25–34.
3. Wu, X.; Cobbina, S.; Mao, G.; Xu, H.; Zhang, Z.; Yang, L. A review of toxicity and mechanisms of individual and mixtures of heavy metals in the environment. *Environ. Sci. Pollut. Res.* **2016**, *23*, 8244–8259. [[CrossRef](#)] [[PubMed](#)]
4. Tchounwou, P.; Yedjou, C.; Patlolla, A.; Sutton, D. Heavy metal toxicity and the environment. In *Molecular, Clinical and Environmental Toxicology*; Springer: Basel, Switzerland; Heidelberg, Germany, 2012; pp. 133–164.
5. Wang, H.; Xu, B.; Liu, J. *Micro and Nano Sulfide Solid Lubrication*; Science Press: Beijing, China, 2012; ISBN 978-7-03-031785-8.
6. Therese, H.A.; Li, J.; Kolb, U.; Tremel, W. Facile Large Scale Synthesis of WS₂ Nanotubes from WO₃ Nanorods Prepared by a Hydrothermal Route. *Solid State Sci.* **2005**, *7*, 67–72. [[CrossRef](#)]
7. Huirache-Acuña, R.; Paraguay-Delgado, F.; Albitzer, M.A.; Alvarez-Contreras, L.; Rivera-Muñoz, E.M.; Alonso-Núñez, G. Synthesis and characterization of WO₃ and WS₂ hexagonal phase nanostructures and catalytic test in sulfur remotion. *J. Mater. Sci.* **2009**, *44*, 4360–4369. [[CrossRef](#)]
8. Kumar, P.; Singh, M.; Gopal, P.; Reddy, G.B. Sulfurization of WO₃ nanorods into WS₂ as a function of H₂S/Ar partial pressure. *AIP Conf. Proc.* **2018**, *1953*, 030252.
9. Perkgoz, N. CVD growth and characterization of 2D transition metal dichalogenides, MoS₂ and WS₂. *Anadolu Univ. J. Sci. Technol. A Appl. Sci. Eng.* **2017**, *18*, 375–387. [[CrossRef](#)]
10. Liu, P.; Luo, T.; Xing, J.; Xu, H.; Hao, H.; Liu, H.; Dong, J. Large-Area WS₂ Film with Big Single Domains Grown by Chemical Vapor Deposition. *Nanoscale Res. Lett.* **2017**, *12*, 558. [[CrossRef](#)] [[PubMed](#)]
11. Hu, S.; Wang, X.; Meng, L.; Yan, X. Controlled synthesis and mechanism of large-area WS₂ flakes by low-pressure chemical vapor deposition. *J. Mater. Sci.* **2017**, *52*, 7215–7223. [[CrossRef](#)]
12. Chen, X.; Wang, X.; Wang, Z.; Yu, W.; Qian, Y. Direct sulfidization synthesis of high-quality binary sulfides (WS₂, MoS₂, and V₅S₈) from the respective oxides. *Mater. Chem. Phys.* **2004**, *87*, 327–331. [[CrossRef](#)]
13. Shang, Y.; Xia, J.; Xu, Z.; Chen, W. Hydrothermal Synthesis and Characterization of Quasi-1-D Tungsten Disulfide Nanocrystal. *J. Dispers. Sci. Technol.* **2005**, *26*, 635–639. [[CrossRef](#)]
14. Shifa, T.A.; Wang, F.; Cheng, Z.; Zhan, X.; Wang, Z.; Liu, K.; Muhammad Safdar, M.; Sun, L.; He, J. Vertical-oriented WS₂ Nanosheet Sensitized by Graphene: An Advanced Electrocatalyst for Hydrogen Evolution Reaction. *Nanoscale* **2015**, *35*, 1–3.
15. Wu, Z.; Wang, D.; Zan, X.; Sun, A. Synthesis of WS₂ nanosheets by a novel mechanical activation method. *Mater. Lett.* **2010**, *64*, 856–858. [[CrossRef](#)]

16. Tang, H.; Zhang, X.; Li, L.; Li, C. Preparation Method of Graphite Alkene Like Tungsten Disulfide Nanometer Sheet. CN Patent 103641173 A, 19 March 2014.
17. Zhang, X.; Xu, H.; Wang, J.; Ye, X.; Lei, W.; Xue, M.; Tang, H.; Li, C. Synthesis of Ultrathin WS₂ Nanosheets and Their Tribological Properties as Lubricant Additives. *Nanoscale Res. Lett.* **2016**, *11*, 442. [[CrossRef](#)] [[PubMed](#)]
18. Zhang, X.H.; Tan, H.; Fan, Z.; Ge, M.Z.; Ye, X.; Xue, M. Synthesis and electrochemical performance of ultrathin WS₂ nanosheets. *Chalcogenide Lett.* **2017**, *14*, 419–423.
19. Stopić, S. *Synthesis of Metallic Nanosized Particles by Ultrasonic Spray Pyrolysis*; Shaker Verlag: Aachen, Germany, 2015; ISBN 978-3844035292.
20. Roine, A. *HSC Chemistry® v 9.0.*; Outotec Research Oy Center: Pori, Finland, 2016.
21. Arutanti, O.; Ogi, T.; Nandiyanto, A.B.; Iskandar, F.; Okuyama, K. Controllable crystallite and particle sizes of WO₃ particles prepared by a spray-pyrolysis method and their photocatalytic activity. *AIChE J.* **2013**, *60*, 41–49. [[CrossRef](#)]
22. Meyer, B. Elemental sulfur. *Chem. Rev.* **1976**, *76*, 367–388. [[CrossRef](#)]
23. Davim, J. (Ed.) *Tribology of Nanocomposites*; Springer: Berlin/Heidelberg, Germany, 2013; ISBN 978-3-642-33882-3.
24. Wu, N.; Hu, N.; Zhou, G.; Wu, J. Tribological properties of lubricating oil with micro/nano-scale WS₂ particles. *J. Exp. Nanosci.* **2018**, *13*, 27–38. [[CrossRef](#)]
25. Aldana, P.U. Tungsten Disulfide Nanoparticles as Lubricant Additives for the Automotive Industry. Ph.D. Thesis, Université de Lyon, Lyon, France, 2016.
26. Nian, J.; Chen, L.; Guo, Z.; Liu, W. Computational investigation of the lubrication behaviors of dioxides and disulfides of molybdenum and tungsten in vacuum. *Friction* **2017**, *5*, 23–31. [[CrossRef](#)]
27. Polcar, T.; Parreira, N.M.G.; Cavaleiro, A. Tungsten oxide with different oxygen contents: Sliding properties. *Vacuum* **2007**, *81*, 1426–1429. [[CrossRef](#)]
28. Çelikbilek Ersundu, M.; Ersundu, A.E.; Sayyed, M.I.; Lakshminarayana, G.; Aydin, S. Evaluation of physical, structural properties and shielding parameters for K₂O-WO₃-TeO₂ glasses for gamma ray shielding applications. *J. Alloys Compd.* **2017**, *714*, 278–286. [[CrossRef](#)]



© 2019 by the authors. Licensee MDPI, Basel, Switzerland. This article is an open access article distributed under the terms and conditions of the Creative Commons Attribution (CC BY) license (<http://creativecommons.org/licenses/by/4.0/>).